crystals

MDPI

Article

Effects of Solvent Vapor Atmosphere on Photovoltaic Performance of Perovskite Solar Cells

Miao He [1,†], Shuyan Chen [1,†], Taoran Wang [2], Gu Xu [3], Na Liu [1,*] and Fan Xu [4,5,*]

[1] Tsinghua-Berkeley Shenzhen Institute, Institute of Materials Science, Tsinghua Shenzhen International Graduate School, Tsinghua University, Shenzhen 518055, China
[2] Energy Materials and Optoelectronics Unit, Songshan Lake Materials Laboratory, China Academy of Sciences, Dongguan 523808, China
[3] Department of Materials Science and Engineering, McMaster University, 1280 Main St. W, Hamilton, ON L8S 4L8, Canada
[4] Frontiers Science Center for Nano-Optoelectronics & Collaborative Innovation Center of Quantum Matter, State Key Laboratory for Artificial Microstructure and Mesoscopic Physics, School of Physics, Peking University, Beijing 100871, China
[5] Shenzhen BTR New Energy Technology Institute Co., Ltd., Shenzhen 518118, China
* Correspondence: nanaliu_nnl@163.com (N.L.); xufan@pku.edu.cn (F.X.)
† These authors contributed equally to this work.

Abstract: Tremendous efforts have been devoted to facilitating the commercialization of perovskite solar cells (PSCs) in the past decade. However, the influence of solvent vapor atmosphere on PSC device performance during its fabrication still lacks related investigations. Here, by using three commonly employed solvent vapors during the perovskite annealing process, i.e., isopropanol, chlorobenzene and dimethylformamide, we reveal the effects of atmosphere on related perovskite film properties and device performance. The results indicate that perovskite films prepared under these external solvent vapors exhibit distinct crystalline phases, morphologies and optical properties from films under normal conditions (nitrogen gas), resulting in a significant drop in power conversion efficiency from the initial 20.01% to the lowest of only ~15%. Our work highlights the importance of atmospheric effects in preparing efficient PSCs for scalable fabrication and commercialization.

Keywords: solvent vapor; atmospheric effects; hybrid perovskites; film crystallizations; solar cells

Citation: He, M.; Chen, S.; Wang, T.; Xu, G.; Liu, N.; Xu, F. Effects of Solvent Vapor Atmosphere on Photovoltaic Performance of Perovskite Solar Cells. *Crystals* **2023**, *13*, 549. https://doi.org/10.3390/cryst13040549

Academic Editor: Ray-Hua Horng

Received: 22 February 2023
Revised: 13 March 2023
Accepted: 21 March 2023
Published: 23 March 2023

1. Introduction

The urgent demands for carbon neutrality require the development and utilization of renewable energy resources such as solar energy [1]. Perovskite solar cells (PSCs) have been recognized as one of the most promising candidates for the next generation of photovoltaics (PV). Benefiting from distinguished advantages [2–5], including low exciton binding energy, high defect tolerance and long diffusion length, the power conversion efficiency (PCE) of PSCs has reached 25.7% within decades, rivaling already the conventional silicon (Si) cells (~26.7%) [6].

It is vital to optimize the crystallization process of the perovskite layer to achieve highly efficient PSCs, as it could directly influence the obtained film morphology and, thus, the device efficiency [7,8]. It has been suggested that perovskites with high crystallinity and uniform morphology tend to exhibit better PV performance [9]. In fact, the crystallization process of perovskites can be affected by various factors, such as solvent types [10–12], external environmental conditions [13,14], precursor compositions [15–18], etc. For example, Seok et al. employed toluene as an antisolvent to retard the crystallization rates of perovskite formation, resulting in enlarged grain sizes and improved PCE [10]. Moreover, other factors such as light [14] and lead anion types [15] were also found to strongly influent the film crystallization kinetics and the obtained film morphology.

In addition to the above efforts, the atmosphere during film fabrication, such as humidity and oxygen, may also affect the perovskite structure and related device performance [19–22]. Currently, most PSCs are fabricated via solution-processed methods, where large amounts of solvents (e.g., isopropanol, dimethylformamide, etc.) need to be used [10]. This will change atmospheric environments that are surrounded by the perovskite film during its preparation. While the essential function of solvents is to dissolve solid precursors, they may also influent the perovskite crystallization process and, thus, the device performance [23–25]. Several previous works in the literature investigated the solvent vapor annealing process in pure $MAPbI_3$-based PSCs [23,26,27]. However, for the most employed FA-based perovskites with the highest PCE, such solvent vapor atmospheric effects have not been unraveled thus far.

It is, therefore, the purpose of the current work to investigate the influence of solvent vapor atmospheres on FA-based perovskite film properties and related device performance. Three commonly employed solvents in PSC investigations, namely isopropanol (IPA), chlorobenzene (CB) and dimethylformamide (DMF), were applied during the film formation process, and their impacts on the film structure, morphology and optical properties were studied and unraveled. To better compare, perovskite films were crystallized in the as-demonstrated atmosphere-controlled apparatus (Figure 1). The results indicate the detrimental effects of such solvent vapors on the perovskite film morphologies and properties, which result in a significant drop of device PCE from 20.01% (control) down to only ~15% (DMF-treated). Our work highlights the importance and necessity of controlling the solvent vapor atmosphere during device fabrication to acquire PSCs with high efficiency.

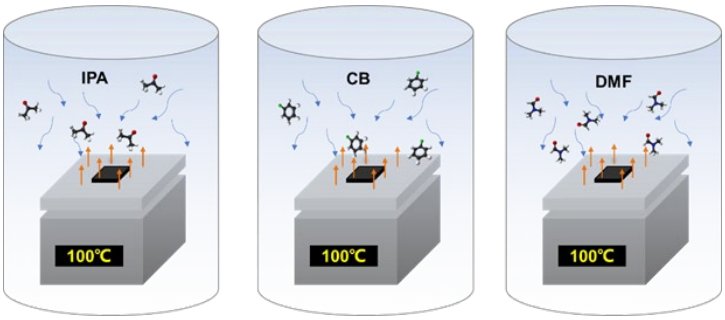

Figure 1. Schematic illustration of the atmosphere-controlled apparatus during perovskite film annealing.

2. Materials and Methods

2.1. Materials

All the commercial materials were used as received without further purification, including ethanol (AR Beijing Chemical Works, Beijing, China), chlorobenzene (99.9%, Sigma-Aldrich, St. Louis, MO, USA), isopropanol (IPA, 99.99%, Sigma-Aldrich, St. Louis, MO, USA), N,N-dimethylformamide (DMF, 99.99%, Sigma-Aldrich, St. Louis, MO, USA), Dimethyl sulfoxide (DMSO, 99.9%, Sigma-Aldrich, St. Louis, MO, USA), Toluene (TL, 99.98%, Sigma-Aldrich, St. Louis, MO, USA), Poly (triarylamine) (PTAA, Xi'an Polymer Light Technology Corp., Xi'an, China), [6,6]-Phenyl C_{61} butyric acid methyl ester ($PC_{61}BM$, Xi'an Polymer Light Technology Corp., Xi'an, China), PbI_2 (99.999%, Xi'an Polymer Light Technology Corp., Xi'an, China), CsI (99.90%, Sigma-Aldrich, St. Louis, MO, USA), Formamidinium iodide (FAI, Xi'an Polymer Light Technology Corp., Xi'an, China).

2.2. Device Fabrication

To prepare the solar cell devices, the ITO substrate was first sequentially washed with distilled water and ethanol twice each. After drying under an electric thermostatic drying oven, the substrates were treated with oxygen plasma treated for 120 s to generate the hydrophilic surface. Then, 2 mg mL^{-1} of PTAA solution (dissolved in toluene) was spin-coated onto ITO

substrates at 5000 rpm for 20 s, followed by annealing at 110 °C for 10 min in a glove box with a Nitrogen atmosphere. After cooling to room temperature, 80 µL perovskite precursor solution (1.05 M $FA_{0.85}Cs_{0.15}PbI_3$ dissolved in 800 µL DMF and 200 µL DMSO) was spin-coated on the PTAA substrates with a spin speed of 1000 rpm for 8 s, and 5000 rpm for the 30 s, 20 s into the 5000 rpm process, 100 µL of CB was deposited onto the substrate, then annealed at 100 °C for 30 min. For solvent vapor-treated samples, a top-sealed glass cylinder was applied to control the surrounding atmosphere during perovskite film annealing (Figure 1). The solvent annealing time is 30 min. To generate solvent vapor, 30 µL of the selected solvent (e.g., IPA, CB, DMF) was pre-added in the cylinder, with the temperature at around 100 °C. After cooling down, 20 mg mL^{-1} of $PC_{61}BM$ solution (dissolved in chlorobenzene) was deposited via spin coating at 2000 rpm for the 30 s onto the perovskite film. Finally, the devices were transferred into a vacuum chamber for the deposition of Ag (100 nm) electrode under a base pressure of 4.0×10^{-4} Pa. The size of the perovskite photoactive layer is 1.5 cm × 1.5 cm. The effective area of each cell was 0.102 cm^2, defined by masks for all PSCs discussed in this work.

2.3. Characterizations

XRD was carried out by an X-ray diffractometer (PANalytical X'pertPRO) equipped with Cu-Kα X-ray tube. Scanning electron microscope (SEM) images were measured on a field emission scanning electron microscope (JEOL-7401). Absorption thin films were recorded on an HP 8453 spectrophotometer. Steady-state photoluminescence (PL) and time-resolved photoluminescence (TRPL) were obtained by using an FLS920 (Edinburgh Instruments Ltd., Edinburgh, Scotland) with an excitation wavelength at 475 nm and 365 nm, respectively. Current density–voltage (J-V) curves were measured by using a 2400 Series Source Meter (Keithley Instruments, Solon, OH, USA) measure unit (Newport, Oriel AM 1.5G, 100 mW cm^{-2}); the accuracy was calibrated by an NREL standard Si cell. The measurements were carried out with the scanned voltage of 1.2 V to −0.2 V (reverse). Incident photon-to-electron conversion efficiencies (IPCE) were determined on a solar cell QE/IPCE measurement system provided by Zolix Co., Ltd., Beijing, China.

3. Results and Discussion

First, we conducted XRD measurements to unravel the structure of perovskite films annealed under different atmospheres, and the results are illustrated in Figure 2. In this work, excessive amounts of PbI_2 were introduced to enhance the device efficiency [28], corresponding to the diffraction peak at ~12.4°. However, such a peak almost disappears in the IPA- and CB-treated films, suggesting the removal of the residue PbI_2. Moreover, an additional peak that occurred at 11.4° further suggests the formation of δ-phase perovskite with a high bandgap in IPA film [29], which is detrimental to achieving highly efficient PSCs. The DMF-treated film shows a much different diffraction pattern than others, with no obvious peak occurring before 25°, which indicates the low crystallinity of the perovskite.

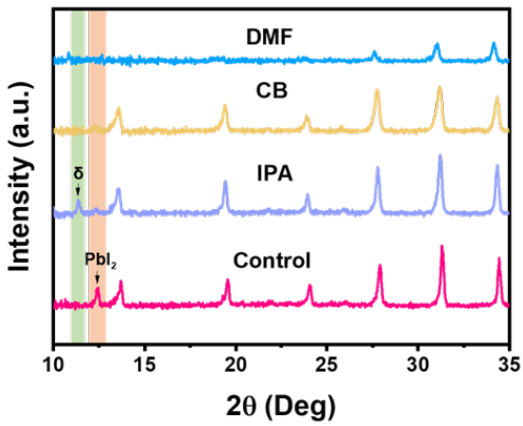

Figure 2. XRD results of perovskite films annealed under different solvent vapors.

Next, to investigate the impacts of different atmospheres on the perovskite film morphology, we measured their planar SEM images (Figure 3). As expected, the controlled film exhibits dense-grain uniform morphology, as well as the largest average grain size, which is consistent with other works [29,30]. Both IPA- and CB-treated films show similar morphologies with smaller grain sizes than the controlled sample, due possibly to the fast evaporation of precursor solvents during the film annealing [12], which will increase the nucleation sites. In contrast, the film fabricated under the DMF atmosphere shows much-increased pinholes/voids at grain boundaries (red circles), which may induce additional shunt paths to increase leakage current losses. Such phenomenon is attributed to the presence of DMF [31], which could re-dissolve the formed perovskites during the film annealing process, resulting in decreased nuclei number and poor film morphology. Furthermore, the cross-section of SEM images for these perovskites was also measured. As shown in Figure S1, the DMF-treated sample exhibited the poorest morphology, which is consistent with planar SEM results.

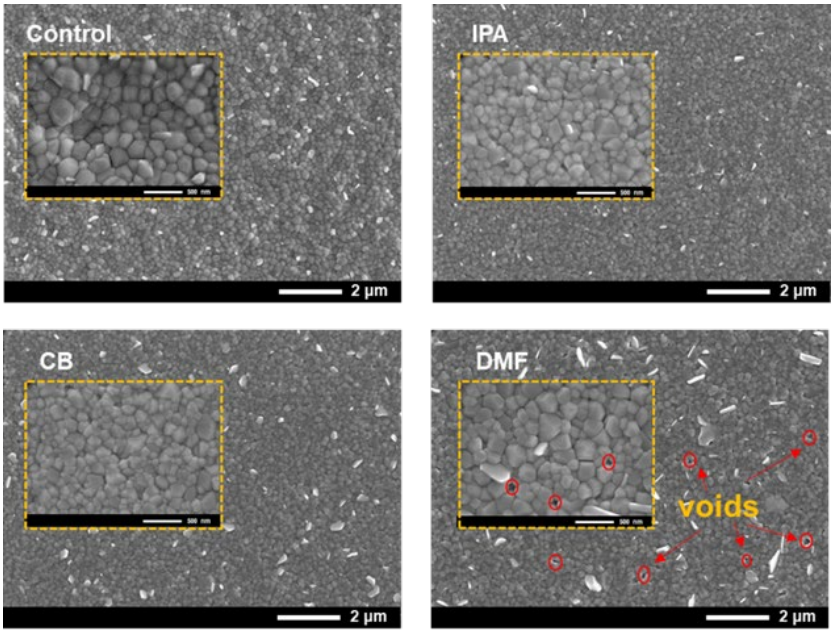

Figure 3. Planar SEM images of perovskites annealed under different atmospheres, with a scale bar of 2 μm. Inset: zoom-in picture, scale bar: 500 nm. All perovskite films were prepared on PTAA-coated ITO glass.

The optical properties of films prepared under different atmospheres were also studied. The absorption results are presented in Figure 4a. Both IPA- and DMF-treated perovskite films show deteriorated absorption between 450 nm and 600 nm, which could be ascribed to the formation of unwanted δ-phase perovskite in IPA-treated film, as well as the poor DMF-treated film coverage on the substrate. In addition, all films exhibit the same absorption onset at ~800 nm, which indicates atmosphere would not affect the bandgap of the perovskite material. This was further confirmed by our steady-state photoluminescence (PL) results (Figure 4b), where four films all show an emission peak at around 795 nm.

Time-resolved photoluminescence (TRPL) measurements were also conducted to investigate charge carrier lifetimes. As illustrated in Figure 4c, the PL decay curves are fitted via the bi-exponential decay model [32]: $y = A_1e^{-x1/\tau1} + A_2e^{-x2/\tau2} + B$. As summarized in Table 1, average charge carrier lifetimes are calculated to be 21.47 ns, 10.14 ns, 13.93 ns and 4.74 ns for the controlled IPA-, CB- and DMF-treated films, respectively. The longest carrier lifetime of the controlled film suggests reduced non-radiative recombination losses, presumably due to the self-passivation effect of PbI_2 [33].

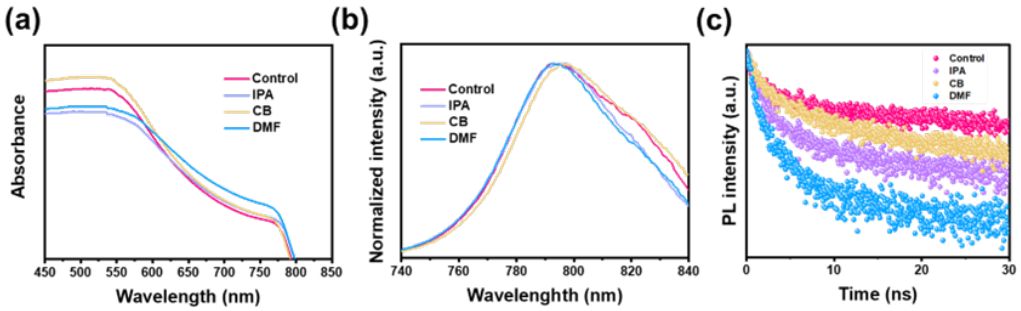

Figure 4. Optical properties of perovskite films under control, IPA, CB and DMF solvent vapor conditions, respectively. (**a**) UV-vis absorption results. (**b**) Steady-state photoluminescence results. (**c**) Time-resolved photoluminescence results. All perovskite films were prepared on PTAA-coated ITO glass.

Table 1. The data for fitted TRPL curves.

	A_1	τ_1 (ns)	A_2	τ_2 (ns)	τ_{ave} (ns)
Control	118.15	23.66	192.52	1.60	21.47
IPA	338.22	1.34	108.59	12.97	10.14
CB	163.85	15.79	231.53	1.70	13.93
DMF	101.67	6.69	354.66	1.00	4.74

To further evaluate the effects of the atmosphere on the PSC's photovoltaic performance, we fabricated a series of solar cells employing the configuration of ITO/PTAA/perovskite/PCBM/Ag. Table 2 shows the distribution results of different PV parameters for devices annealed under various atmospheres. As can be observed, the controlled devices exhibit the highest average PCE, open circuit voltage (V_{OC}) and fill factor (FF) of 19.42%, 1.08 V and 0.78, respectively. Interestingly, the CB-treated PSCs show the best average short circuit current density (J_{SC}) of over 24.29 mA/cm^2. However, the low V_{OC} (~0.99 V) strongly limits their efficiency. Both IPA- and DMF-treated solar cells exhibit deteriorated PV performance due to the existence of unwanted yellow phases and high defect densities, as suggested by the above XRD and TRPL results.

Table 2. Photovoltaic parameters of the controlled, IPA-, CB- and DMF-treated PSCs under one sun illumination.

	V_{OC} (V)	FF	J_{SC} (mA/cm^2)	PCE (Best) (%)	PCE (Average) (%)
Control	1.08	78.01	23.62	20.01	19.42
IPA	1.05	78.58	22.82	18.91	18.46
CB	1.02	78.61	24.32	19.40	18.77
DMF	1.00	76.75	20.77	16.00	15.05

The best JV curves of cells prepared under four different atmospheres are illustrated in Figure 5. The controlled cell exhibits the champion efficiency of 20.01%, with V_{OC}, J_{SC} and FF of 1.08 V, 23.62 mA/cm^2 and 0.78, respectively. A large number of pinholes/voids that existed in DMF-treated devices dramatically decreased the shunt resistance, resulting in the lowest photocurrent density (J_{SC} = 20.77 mA/cm^2) and efficiency. The best CB-treated PSC, on the other hand, shows an unsatisfied V_{OC} of 1.02 V, which might be ascribed to the lack of self-passivated PbI_2 and higher defect density, significantly dropping the photovoltage and efficiency [28]. In previous work, IPA was employed to enhance the crystallinity of $MAPbI_3$ films [23]. However, in FA-based perovskite, it was found that IPA could trigger the undesirable α-to-δ phase transition, which increases the pristine material's bandgap and lowing the charge carrier mobility [34], resulting in deteriorated device PCE. The IPCE

curves for these PSCs were also measured (Figure 5b), where CB- and DMF-treated samples exhibited the highest and lowest current, respectively, corresponding well to the JV results.

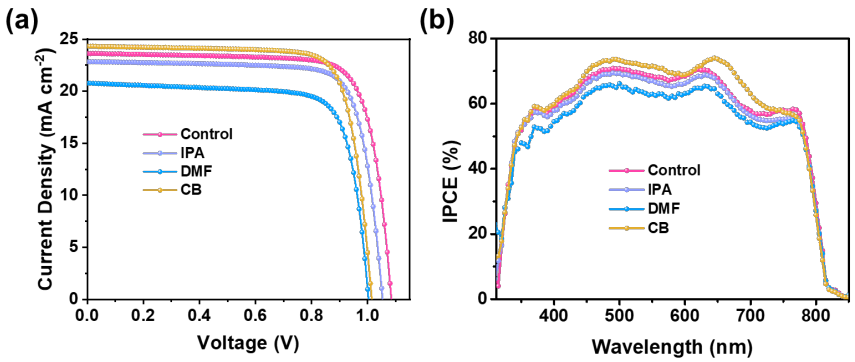

Figure 5. (**a**) The best JV curves and (**b**) IPCE curves of PSCs fabricated under different atmospheres.

4. Conclusions

In summary, the effects of three commonly employed solvent vapors, including IPA, CB and DMF, on the perovskite film properties and related device performance were investigated. It was found that CB could alter the self-passivated perovskite structure by removing its residue PbI_2, thus dropping the device photovoltage. Additionally, annealing the film under IPA induced undesirable δ-perovskite, which will deteriorate the film morphology and optical properties. Notably, the DMF-treated film exhibits the poorest crystallinity and film quality, which might increase the leakage current loss. As a result, PSCs fabricated under normal conditions (control) show the best photovoltaic performance with a PCE of 20.01%. This work highlights the significance of controlling solvent vapor atmosphere during perovskite annealing, in particular for volatile solvents. Hopefully, these discoveries will be able to provide essential guidance for achieving efficient and stable PSCs.

Supplementary Materials: The following supporting information can be downloaded at: https://www.mdpi.com/article/10.3390/cryst13040549/s1, Figure S1: Cross-sectional SEM images of perovskites annealed under different atmospheres, with a scale bar of 500 nm.

Author Contributions: Conceptualization, N.L. and F.X.; methodology, M.H. and S.C.; validation, M.H. and S.C.; investigation, N.L. and F.X.; writing—original draft preparation, F.X.; writing—review and editing, T.W., G.X. and N.L.; supervision, G.X., N.L. and F.X.; project administration, N.L. and F.X.; funding acquisition, G.X., N.L. and F.X. All authors have read and agreed to the published version of the manuscript.

Funding: This research was funded by the Natural Sciences and Engineering Research Council of Canada, Grant Number: RGPIN-2015-05740; National Natural Science Foundation of China, Grant Number: 03012800001; Shenzhen Science and Technology Innovation Committee, Grant Number: JCYJ20190809172615277; Guangdong Basic and Applied Basic Research Foundation, Grant Number: 2020A1515111065.

Data Availability Statement: Not applicable.

Acknowledgments: The authors acknowledge the support from Guangdong Overseas Young Talented Postdoctoral Researcher Project.

Conflicts of Interest: The authors declare no conflict of interest.

References

1. Xu, F.; Li, Y.; Liu, N.; Han, Y.; Zou, M.; Song, T. 1D Perovskitoid as Absorbing Material for Stable Solar Cells. *Crystals* **2021**, *11*, 241. [CrossRef]
2. Yin, W.J.; Shi, T.; Yan, Y. Unique properties of halide perovskites as possible origins of the superior solar cell performance. *Adv. Mater.* **2014**, *26*, 4653–4658. [CrossRef]

3. Yin, W.-J.; Yang, J.-H.; Kang, J.; Yan, Y.; Wei, S.-H. Halide perovskite materials for solar cells: A theoretical review. *J. Mater. Chem. A* **2015**, *3*, 8926–8942. [CrossRef]
4. Xu, A.F.; Wang, R.T.; Yang, L.W.; Liu, E.E.; Xu, G. An Environmentally Stable Organic–Inorganic Hybrid Perovskite Containing Py Cation with Low Trap-State Density. *Crystals* **2020**, *10*, 272. [CrossRef]
5. Du, C.-S.; Ho, I.-H.; Huang, Y.-J.; Lee, R.-H. Quaternary ammonium halide-containing cellulose derivatives for defect passivation in MAPbI 3-based perovskite solar cells. *Sustain. Energy Fuels* **2022**, *6*, 3349–3362. [CrossRef]
6. Xu, F.; Zhang, M.; Li, Z.; Yang, X.; Zhu, R. Challenges and Perspectives toward Future Wide-Bandgap Mixed-Halide Perovskite Photovoltaics. *Adv. Energy Mater.* **2023**, 2203911. [CrossRef]
7. Qin, M.; Chan, P.F.; Lu, X. A Systematic Review of Metal Halide Perovskite Crystallization and Film Formation Mechanism Unveiled by In Situ GIWAXS. *Adv. Mater.* **2021**, *33*, e2105290. [CrossRef]
8. Wang, R.T.; Liu, E.E.; Xu, A.F.; Yang, L.W.; Chen, J.Y.; Xu, G. Ethylammonium Lead Iodide Formation in MAPbI3 Precursor Solutions by DMF Decomposition and Organic Cation Exchange Reaction. *Crystals* **2020**, *10*, 162. [CrossRef]
9. Sharenko, A.; Toney, M.F. Relationships between lead halide perovskite thin-film fabrication, morphology, and performance in solar cells. *J. Am. Chem. Soc.* **2016**, *138*, 463–470. [CrossRef]
10. Jeon, N.J.; Noh, J.H.; Kim, Y.C.; Yang, W.S.; Ryu, S.; Seok, S.I. Solvent engineering for high-performance inorganic–organic hybrid perovskite solar cells. *Nat. Mater.* **2014**, *13*, 897–903. [CrossRef]
11. Seo, Y.-H.; Kim, E.-C.; Cho, S.-P.; Kim, S.-S.; Na, S.-I. High-performance planar perovskite solar cells: Influence of solvent upon performance. *Appl. Mater. Today* **2017**, *9*, 598–604. [CrossRef]
12. Taylor, A.D.; Sun, Q.; Goetz, K.P.; An, Q.; Schramm, T.; Hofstetter, Y.; Litterst, M.; Paulus, F.; Vaynzof, Y. A general approach to high-efficiency perovskite solar cells by any antisolvent. *Nat. Commun.* **2021**, *12*, 1878. [CrossRef] [PubMed]
13. Dualeh, A.; Tétreault, N.; Moehl, T.; Gao, P.; Nazeeruddin, M.K.; Grätzel, M. Effect of annealing temperature on film morphology of organic–inorganic hybrid pervoskite solid-state solar cells. *Adv. Funct. Mater.* **2014**, *24*, 3250–3258. [CrossRef]
14. Ummadisingu, A.; Steier, L.; Seo, J.-Y.; Matsui, T.; Abate, A.; Tress, W.; Grätzel, M. The effect of illumination on the formation of metal halide perovskite films. *Nature* **2017**, *545*, 208–212. [CrossRef]
15. Moore, D.T.; Sai, H.; Tan, K.W.; Smilgies, D.-M.; Zhang, W.; Snaith, H.J.; Wiesner, U.; Estroff, L.A. Crystallization kinetics of organic–inorganic trihalide perovskites and the role of the lead anion in crystal growth. *J. Am. Chem. Soc.* **2015**, *137*, 2350–2358. [CrossRef]
16. Jeon, N.J.; Noh, J.H.; Yang, W.S.; Kim, Y.C.; Ryu, S.; Seo, J.; Seok, S.I. Compositional engineering of perovskite materials for high-performance solar cells. *Nature* **2015**, *517*, 476–480. [CrossRef]
17. Yang, X.; Li, Q.; Zheng, Y.; Luo, D.; Zhang, Y.; Tu, Y.; Zhao, L.; Wang, Y.; Xu, F.; Gong, Q.; et al. Perovskite hetero-bilayer for efficient charge-transport-layer-free solar cells. *Joule* **2022**, *6*, 1277–1289. [CrossRef]
18. Haris, M.P.; Kazim, S.; Ahmad, S. Low-temperature-processed perovskite solar cells fabricated from presynthesized CsFAPbI3 powder. *ACS Appl. Energy Mater.* **2021**, *4*, 2600–2606. [CrossRef]
19. Sheikh, A.D.; Bera, A.; Haque, M.A.; Rakhi, R.B.; Del Gobbo, S.; Alshareef, H.N.; Wu, T. Atmospheric effects on the photovoltaic performance of hybrid perovskite solar cells. *Sol. Energy Mater. Sol. Cells* **2015**, *137*, 6–14. [CrossRef]
20. Tai, Q.; You, P.; Sang, H.; Liu, Z.; Hu, C.; Chan, H.L.; Yan, F. Efficient and stable perovskite solar cells prepared in ambient air irrespective of the humidity. *Nat. Commun.* **2016**, *7*, 11105. [CrossRef]
21. Wang, R.T.; Xu, A.F.; Chen, J.Y.; Yang, L.W.; Xu, G.; Jarvis, V.; Britten, J.F. Reversing Organic–Inorganic Hybrid Perovskite Degradation in Water via pH and Hydrogen Bonds. *J. Phys. Chem. Lett.* **2019**, *10*, 7245–7250. [CrossRef] [PubMed]
22. Wang, R.T.; Xu, A.F.; Li, W.; Li, Y.; Xu, G. Moisture-Stable FAPbI3 Perovskite Achieved by Atomic Structure Negotiation. *J. Phys. Chem. Lett.* **2021**, *12*, 5332–5338. [CrossRef] [PubMed]
23. Sun, X.; Zhang, C.; Chang, J.; Yang, H.; Xi, H.; Lu, G.; Chen, D.; Lin, Z.; Lu, X.; Zhang, J. Mixed-solvent-vapor annealing of perovskite for photovoltaic device efficiency enhancement. *Nano Energy* **2016**, *28*, 417–425. [CrossRef]
24. Wang, P.; Lü, W.; Wang, M.; Yang, L.; Wang, F.; Liu, H.; Wei, M.; Yang, J.; Fan, L. Novel insights into the role of solvent environment in perovskite solar cells prepared by two-step sequential deposition. *J. Power Sources* **2020**, *480*, 228862. [CrossRef]
25. Liu, T.; Dong, X.; Li, J.; Liu, H.; Wang, S.; Li, X. Effect of concomitant anti-solvent engineering on perovskite grain growth and its high efficiency solar cells. *Sci. China Mater.* **2021**, *64*, 267–276. [CrossRef]
26. Eze, V.O.; Seike, Y.; Mori, T. Synergistic effect of additive and solvent vapor annealing on the enhancement of MAPbI3 perovskite solar cells fabricated in ambient air. *ACS Appl. Mater. Interfaces* **2020**, *12*, 46837–46845. [CrossRef]
27. Zhong, Y.; Seeberger, D.; Herzig, E.M.; Köhler, A.; Panzer, F.; Li, C.; Huettner, S. The impact of solvent vapor on the film morphology and crystallization kinetics of lead Halide perovskites during annealing. *ACS Appl. Mater. Interfaces* **2021**, *13*, 45365–45374. [CrossRef]
28. Chen, Q.; Zhou, H.; Song, T.-B.; Luo, S.; Hong, Z.; Duan, H.-S.; Dou, L.; Liu, Y.; Yang, Y. Controllable self-induced passivation of hybrid lead iodide perovskites toward high performance solar cells. *Nano Lett.* **2014**, *14*, 4158–4163. [CrossRef]
29. Xu, A.F.; Liu, N.; Xie, F.; Song, T.; Ma, Y.; Zhang, P.; Bai, Y.; Li, Y.; Chen, Q.; Xu, G. Promoting thermodynamic and kinetic stabilities of FA-based perovskite by an in situ bilayer structure. *Nano Lett.* **2020**, *20*, 3864–3871. [CrossRef]
30. Liu, N.; Du, Q.; Yin, G.; Liu, P.; Li, L.; Xie, H.; Zhu, C.; Li, Y.; Zhou, H.; Zhang, W.-B. Extremely low trap-state energy level perovskite solar cells passivated using NH 2-POSS with improved efficiency and stability. *J. Mater. Chem. A* **2018**, *6*, 6806–6814. [CrossRef]

31. Zheng, L.; Zhang, D.; Ma, Y.; Lu, Z.; Chen, Z.; Wang, S.; Xiao, L.; Gong, Q. Morphology control of the perovskite films for efficient solar cells. *Dalton Trans.* **2015**, *44*, 10582–10593. [CrossRef] [PubMed]
32. Zhao, L.; Li, Q.; Hou, C.-H.; Li, S.; Yang, X.; Wu, J.; Zhang, S.; Hu, Q.; Wang, Y.; Zhang, Y. Chemical Polishing of Perovskite Surface Enhances Photovoltaic Performances. *J. Am. Chem. Soc.* **2022**, *144*, 1700–1708. [CrossRef] [PubMed]
33. Zhang, D.; Zhang, H.; Guo, H.; Ye, F.; Liu, S.; Wu, Y. Stable α-FAPbI3 in inverted perovskite solar cells with efficiency exceeding 22% via a self-passivation strategy. *Adv. Funct. Mater.* **2022**, *32*, 2200174. [CrossRef]
34. Marchenko, E.I.; Fateev, S.A.; Korolev, V.V.; Buchinskiy, V.; Eremin, N.; Goodilin, E.A.; Tarasov, A.B. Structure-related bandgap of hybrid lead halide perovskites and close-packed APbX 3 family of phases. *J. Mater. Chem. C* **2022**, *10*, 16838–16846. [CrossRef]